



Citation for published version:

Xu, Z., Xie, M., Kim, J.E., Huda, N., Gao, Z., Li, G. & Luo, W. 2020, 'Emerging investigator series: Onsite recycling of saline-alkaline soil washing water by forward osmosis: Techno-economic evaluation and implication', *Environmental Science: Water Research and Technology*, vol. 6, no. 10, pp. 2881-2890.
<https://doi.org/10.1039/d0ew00490a>

DOI:

[10.1039/d0ew00490a](https://doi.org/10.1039/d0ew00490a)

Publication date:

2020

Document Version

Peer reviewed version

[Link to publication](#)

University of Bath

Alternative formats

If you require this document in an alternative format, please contact:
openaccess@bath.ac.uk

General rights

Copyright and moral rights for the publications made accessible in the public portal are retained by the authors and/or other copyright owners and it is a condition of accessing publications that users recognise and abide by the legal requirements associated with these rights.

Take down policy

If you believe that this document breaches copyright please contact us providing details, and we will remove access to the work immediately and investigate your claim.

1 **Engineering Membrane Distillation with**
2 **Nanofabrication: Design, Performance and**
3 **Mechanisms**

4
5 *Environmental Science: Water Research and Technology*

6 Revised: 20 April, 2020

7 Rui Huang ^{1,2}, Zhiqian Liu ³, Yun Chul Woo ^{4,5}, Wenhai Luo ^{6,7}, Stephen R. Gray⁸, Ming Xie ^{1*}

8 ¹ Department of Chemical Engineering, University of Bath, Bath, BA2 7AY, United Kingdom

9 ² School of Environment, Harbin Institute of Technology, Harbin 150090, China

10 ³ Key Laboratory for Water Quality and Conservation of the Pearl River Delta, Ministry of
11 Education; Institute of Environmental Research at Greater Bay, Guangzhou University,
12 Guangzhou 510006, China

13 ⁴ Department of Land, Water, and Environment Research, Korea Institute of Civil Engineering
14 and Building Technology (KICT), 283, Goyang-Daero, Ilsanseo-Gu, Goyang-Si, Gyeonggi-Do,
15 10223, Republic of Korea

16 ⁵ Department of Civil and Environment Engineering, University of Science and Technology
17 (UST), 217, Gajeong-Ro, Yuseong-Gu, Daejeon, 34113, Republic of Korea

18 ⁶ Sustainable Energy Systems Engineering Group, School of Engineering, Macquarie University,
19 Sydney, NSW, 2109, Australia

20 ⁷ Beijing Key Laboratory of Farmland Soil Pollution Prevention and Remediation, College of
21 Resources and Environmental Sciences, China Agricultural University, Beijing 100193, China

22 ⁸ Institute for Sustainable Industries and Liveable Cities, Victoria University, Melbourne, 8001,
23 Australia

24
25
26
27 *Corresponding author. E-mail: mx406@bath.ac.uk

28

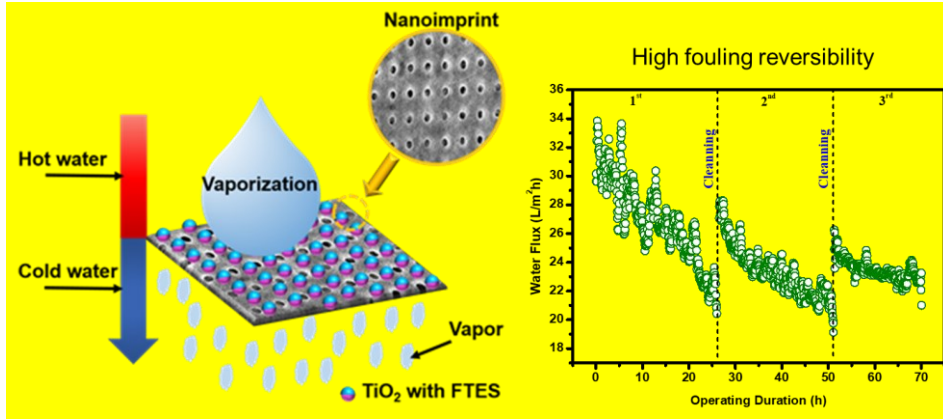
29 **ABSTRACT**

30 Anti-fouling and durability are two important parameters that are closely associated with
31 the development and deployment of membrane distillation (MD). In this study, we reported a
32 nanoimprinted, omniphobic polytetrafluoroethylene (PTFE) membrane with hierarchical rough
33 structure for MD process. A highly ordered, circular surface pattern was first imparted to PTFE
34 membrane substrate via nanoimprint technique. An ultra-thin TiO₂ layer was deposited onto the
35 nanoimprinted membrane to create spherical hierarchical rough structure via atomic layer
36 deposition as well as initiator for chemical fluorination of the membrane. The resultant,
37 nanofabricated membrane exhibited a water contact angle of 155° and contact angle above 100°
38 against a range of low surface tension liquids. In addition, the nanofabricated membrane
39 displayed a high and stable water flux around 34 Lm⁻²h⁻¹ for more than 24 hours, and nearly
40 complete salts rejection with the presence of surfactant. Most importantly, the water flux
41 recovery rate of the resultant membrane was more than 91.3% after three fouling-cleaning
42 cycles, demonstrating an excellent fouling reversibility. The new strategy proposed here that
43 combines nanoimprint technique and super-hydrophobic modification sheds light into
44 developing MD membrane with considerable durability and anti-fouling performance.

45 **Water Impact Statement**

46 Membrane distillation (MD) holds promise for sustainable brine management. To achieve this
47 goal, we presented a facile and green approach for MD membrane design combining
48 nanofabrication and chemical modification. The resultant MD membrane demonstrated anti-
49 wetting and high fouling reversibility in treatment of brine waste containing surfactant and
50 foulants.

51 **Graphical Abstract**



53 1. Introduction

54 Nowadays, water crisis has become an increasing concern all over the world due to severe
55 water pollution and freshwater scarcity¹⁻³. Although around 70% of the earth is covered by water,
56 fresh water only accounts for 0.3%⁴. Therefore, it is imperative to develop reliable and economic
57 technologies to treat seawater as an alternative source. Membrane distillation (MD), developed in
58 recent decades, is a promising technology for seawater desalination and particularly for brine
59 management and zero liquid discharge⁵⁻⁷. It is driven by the vapour pressure difference existing
60 between the porous membrane surfaces, in which only vapour molecules are able to pass through
61 the membrane⁸. Moreover, the heat energy that drive MD process could come from industrial
62 waste heat⁹. Thus, MD is emerging as a viable technology for the desalination of seawater.

63 Membrane wetting is a primary barrier to widespread industrial use of MD, which is caused
64 by partial or complete blocking of pores by liquid-phase water on the feed side^{10, 11}. As a result,
65 membranes for MD are usually fabricated using hydrophobic polymers, such as polyvinylidene
66 fluoride (PVDF)¹², polypropylene (PP)¹³, and polytetrafluoroethylene (PTFE)¹⁴, to prevent
67 wetting. Increasing membrane surface hydrophobicity could reduce capillary attraction of water
68 into the membrane pore, thereby mitigating pore wetting¹⁵. Inspired by the feature of lotus leaf or
69 sharkskin, super-hydrophobic membranes were first tailored by constructing a hierarchical rough
70 structure combined with hydrophobic surface¹⁶⁻¹⁸. Hydrophobic surfaces with hierarchical rough
71 structure can provide air pockets that decrease the total contact area between the membrane and
72 water¹⁹. Grafting or mixing with low surface energy materials, such as fluoroalkyl-chains, on
73 membrane surface is another common method to increase hydrophobicity²⁰.

74 Increasing surface hydrophobicity could however exacerbate membrane fouling. Because of
75 strong hydrophobic-hydrophobic interactions, hydrophobic foulants can easily attach to the
76 hydrophobic membrane surface and wick into the membrane pores, and thus adversely converts
77 vapour transportation to direct liquid intrusion into the membrane pore²¹. To overcome this
78 contradiction, researchers have developed Janus membranes with asymmetric wettability in more
79 recent years^{22, 23}. The outmost layer of Janus membranes is super-hydrophilic, which is designed
80 to prevent mass transfer of foulants like micro oil drops. For example, Zhu et al.²⁴ developed a
81 hydrophobic PVDF fibrous membrane substrate with a hydrophilic SiO₂/PAN skin layer,

82 demonstrating its stable performance in the treatment of high-salinity water containing a high
83 concentration of lubricating oil. Nevertheless, these Janus membranes are much more difficult to
84 tailor. Most of them suffer sacrificed breathability (water vapour transmission)^{22, 25}. Thus, a
85 simple method to construct both anti-wetting and anti-fouling MD membranes for the efficient
86 desalination is required.

87 Nanoimprint, a simple and versatile nanofabrication technique, has been proposed for
88 membrane fabrication^{26, 27}, which endows membrane surface with highly ordered features and
89 thus can mitigate membrane fouling. Our previous study has proven that the PTFE membrane
90 with periodical line pattern could significantly mitigate membrane fouling in MD process²⁸, due
91 to significantly low adhesion force between foulants and patterned MD membrane surface.
92 However, the durability of pristine PTFE nanoimprinted membranes was still unsatisfactory.
93 Therefore, combining the nanoimprint technique with super-hydrophobic modification would
94 have great potential to address wetting and fouling problems in MD process.

95 Herein, we presented a nanoimprinted, omniphobic membrane via nanoimprint technique,
96 atomic layer deposition and fluorination, with the expectation to mitigate both membrane wetting
97 and fouling. The fabricated membrane had a periodical circle pattern with hierarchical rough
98 structure and low surface energy. The morphologies and chemical properties of the membrane
99 were systematically characterized. Sodium dodecyl sulfate (SDS) and humic acid were chosen as
100 the model contaminants to evaluate the durability and anti-fouling performance of the
101 membrane. The green and facial method used here may be a potential candidate for brine
102 management with complex compositions and varying foulants.

103

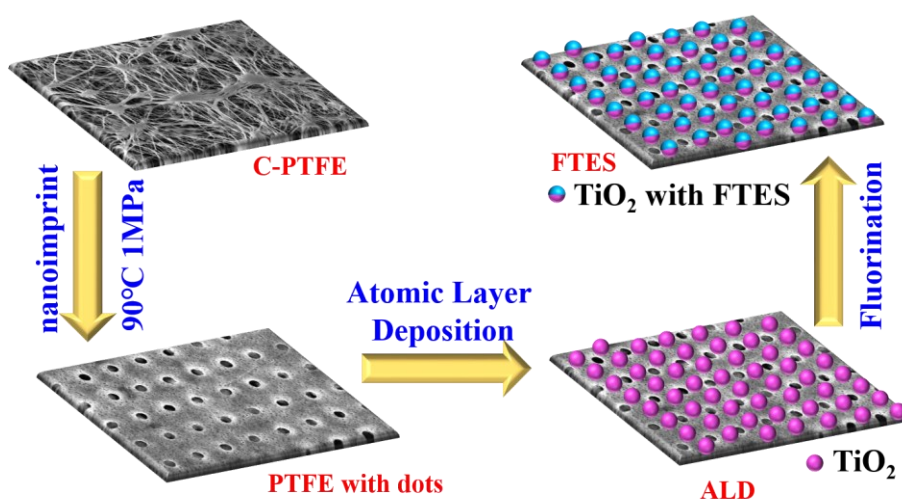
104 **2. Materials and methods**

105 **2.1 Nanofabrication for membrane distillation**

106 Nanofabrication was employed to engineer commercially available PTFE membrane
107 (Durapore, 0.4 μm pore size, 280 μm thickness) with nanoimprint, atomic layer deposition of
108 TiO_2 and fluorination by FTES (1H,1H,2H,2H-perfluorooctyltriethoxysilane) in tandem (Figure

109 1). The resultant membrane in the aforementioned procedure was denoted as C-PTFE, ALD and
110 FTES, respectively.

111 ALD, as a thin film deposition technique, can control the thickness of thin films at the
112 angstrom level based on sequential self-limiting, gas-solid surface reactions²⁹. From deposition
113 chemistry perspective, ALD proceeds via two half-reactions where reactants (precursors) are
114 pulsed into reactor alternately and cycle-wise; while CVD is a continuous process where all
115 reactants are supplied at the same time to grow the film. Another feature of ALD is that it is
116 capable of low-temperature processing³⁰ compared to CVD deposition techniques, thereby being
117 suitable for processing polymeric membranes.



118
119 **Figure 1:** Schematic illustration of design and procedures for fabricating nanoimprint PTFE
120 membrane with fluorinated TiO₂ deposition layer.

121 The PTFE membrane was first imparted with surface pattern by nanoimprinter (EVG 510,
122 Thallner GmbH, Germany). Specifically, the PVDF membrane was placed on nickel substrate to
123 ensure an even temperature. The silicon mask used possessed dot pattern with circle diameter of
124 6 μm and spacing (edge-to-edge) of 6 μm (Figure S1, Supplementary Data). The silicon mask
125 was cleaned with acetone prior to the fabrication to clean off any debris from previous use.
126 Patterning was carried out at 90 °C with a pressure of 1 MPa for 120 s, and the silicon mask was
127 separated from the membrane samples at 35 °C. The pressure (i.e., piston force) and temperature
128 were closely monitored during the nanoimprint to ensure sufficient surface patterns.

129 After nanoimprinting, we deposited an ultrathin layer of TiO₂ (around 5 nm in thickness)
130 on the dot patterned MD membrane by atomic layer deposition (Fiji F200 ALD, Cambridge
131 Nanotech). Tetrakis(dimethylamino) titanium (Strem Chemicals, Inc., USA), as known as
132 TDMAT, and H₂O vapour were used as titanium and oxygen precursors, respectively. An ALD
133 growth cycle of TiO₂ deposition consisted of the following steps and parameters: TDMAT pulse
134 0.1 s, N₂ purge 8 s, H₂O pulse 60 ms, N₂ purge 8s, deposition temperature at 120 °C. The total
135 cycle of TiO₂ deposition was 125, resulting in TiO₂ thickness around 5 nm. The actual thickness
136 of TiO₂ was estimated using a reference silicon wafer by a variable angle spectroscopic
137 ellipsometer (J.A. Woollam M-2000DI).

138 Utilising the ultrathin film of TiO₂ on dot patterned MD membrane, we further
139 functionalised it with FTES (1H, 1H, 2H, 2H-perfluorooctyltriethoxysilane). Specifically,
140 hydroxylated FTES in toluene were prepared in 50 mL bottles through sonication and vigorous
141 stirring for one hour, respectively. The coating procedure occurred in a glove box over 18 hours
142 to obtain the resultant membrane, which was then washed with toluene and completely dried in
143 an oven prior to use.

144

145 **2.2 Membrane distillation apparatus and filtration protocol**

146 Direct contact membrane distillation (DCMD) was conducted using a closed-loop bench-
147 scale membrane test apparatus. The membrane cell was made of acrylic plastic to minimize heat
148 loss to the surroundings. The flow channels were engraved in each of two acrylic blocks that
149 made up the feed and permeate semi-cells. Each channel was 0.2 cm deep, 1.5 cm wide, and 1.5
150 cm long; and the total active membrane area was 2.25 cm². Temperatures of feed and distillate
151 solutions were controlled by two heater/chillers (Polyscience, IL, USA), and were continuously
152 recorded by temperature sensors that were inserted at the inlet and outlet of the membrane cell.
153 Both feed and distillate streams were concurrently circulated by two gear pumps. The same
154 crossflow rate of 30 L h⁻¹ (corresponding to the crossflow velocity of 9 cm s⁻¹) was applied to
155 both feed and distillate in order to minimize the pressure difference across the MD membrane.
156 Weight change of the distillate tank was recorded by an electronic balance (Mettler Toledo, OH,

157 USA) with a data logger. All piping used in the DCMD test unit was covered with insulation
158 foam to minimize heat loss.

159 The nanofabricated MD membrane was subject to both wetting and fouling experiments.
160 Specifically, MD membrane wetting and fouling were simulated with feed solution containing 70
161 g L⁻¹ NaCl solution (simulating seawater brine from reverse osmosis) with either 1 mM sodium
162 dodecyl sulfate (SDS) or 50 mg L⁻¹ humic acid, respectively. In addition, MD membrane
163 fouling-cleaning cycle was conducted three times in order to examine the fouling reversibility
164 and cleaning efficiency by physical flushing. In the cleaning mode, the humic acid fouled MD
165 membrane was flushed by DI water at doubled cross flow rate (i.e., 18 cm s⁻¹) for 20 min. After
166 this brief, physical flushing, the fouling filtration resumed.

167 Feed and distillate volumes of four and one litre were used, respectively. Temperature of
168 inlet feed solution was 60 °C; while that of the distillate inlet stream was 20 °C in all
169 experiments. A new membrane sample was used for each experiment. Permeate mass was
170 recorded by a digital balance continuously. Conductivity of the distillate was measured by a
171 conductivity meter (HQ14d, Hach, CO) every 5 minutes.

172

173 **2.3 Characterization of nanofabricated membrane**

174 The nanofabricated MD membrane was comprehensively characterized in order to gain
175 insights in structure-performance relationship. Scanning electron microscopy (SEM), Fourier
176 transform infrared spectroscopy (FTIR), X-ray photoelectron spectroscopy (XPS), atomic force
177 microscopy (AFM) and thermo-gravimetric analysis (TGA) were employed to analyze the
178 morphology, thermal and physicochemical properties of the nanofabricated MD membrane.

179 Surface and cross-section morphology of the completely dried membranes with the gold
180 coating was visualized by EVO MA 10 (Zeiss, Germany) scanning electron microscope at an
181 accelerating voltage of 20 kV. AFM images were acquired with an Asylum Research MFP-3D
182 AFM operating in intermittent contact (“tapping”) mode with a Budget Sensors TAP150Al-G
183 cantilever ($f_R = 123$ kHz, $Q = 1745$ and $k = 2.1$ Nm⁻¹, with free-air amplitude = 100 nm and
184 feedback set-point = 70 %).

185 To obtain information about composition and bonding chemistry of the MD membrane
186 surface layer (with penetration depth from 1 to 5 nm thickness), X-ray photoelectron
187 spectroscopy (XPS) analysis was carried out on monochromatic aluminium $K\alpha$ X-ray
188 photoelectron spectrometer (Thermo Scientific, MA). Survey spectra were recorded 3 times per
189 sample, over the range of 0-1000 at 1 eV resolution to analyse the elemental composition.
190 Bonding chemistry of membrane surface layer was analysed by high resolution C1s scan with
191 XPS. A spot size of 400 μm was used to scan in the region of the C1s binding energy at 20 eV
192 pass energy. Two random spots on duplicate membrane samples were selected. Excessive
193 charging of samples was minimized using an electron flood gun. High resolution scans had a
194 resolution of 0.1 eV. Calibration for the elemental binding energy was done based on the
195 reference for carbon 1s at 284.6 eV. Data were processed by standard software with Shirley
196 background and relative sensitivity factor of 0.278 for C1s peaks.

197 Membrane surface functional groups were identified using a Fourier Transform Infrared
198 (FTIR) spectrometer (Thermo Scientific Nicolet 6700) equipped with an ATR accessory
199 consisting of a ZnSe plate (45° angle of incidence). Absorbance spectra were measured with 64
200 scans of each sample at a spectral resolution of 2 cm^{-1} . Background measurements in air were
201 collected before each membrane sample measurement. ATR-FTIR spectra were collected at two
202 different spots for each membrane sample.

203 Membrane contact angle (CA) was measured by the sessile drop method using an optical
204 subsystem (Theta Lite 100) integrated with an image-processing software. A range of liquids
205 (water, diiodomethane, ethylene glycol and ethanol) were used for contact angle measurement.³¹

206 Thermal property of the nanofabricated MD membrane was quantified by thermo-
207 gravimetric analysis (TGA) (Discovery TGA thermo-gravimetric analyser, SDT-Q600, United
208 States) from $50\text{ }^\circ\text{C}$ to $700\text{ }^\circ\text{C}$ at a heating rate of $10\text{ }^\circ\text{C}/\text{min}$ in N_2 atmosphere. The crucible
209 material was platinum. Each sample was dried by purging N_2 for 1 min before measurement.

210

211 **3. Results and Discussion**

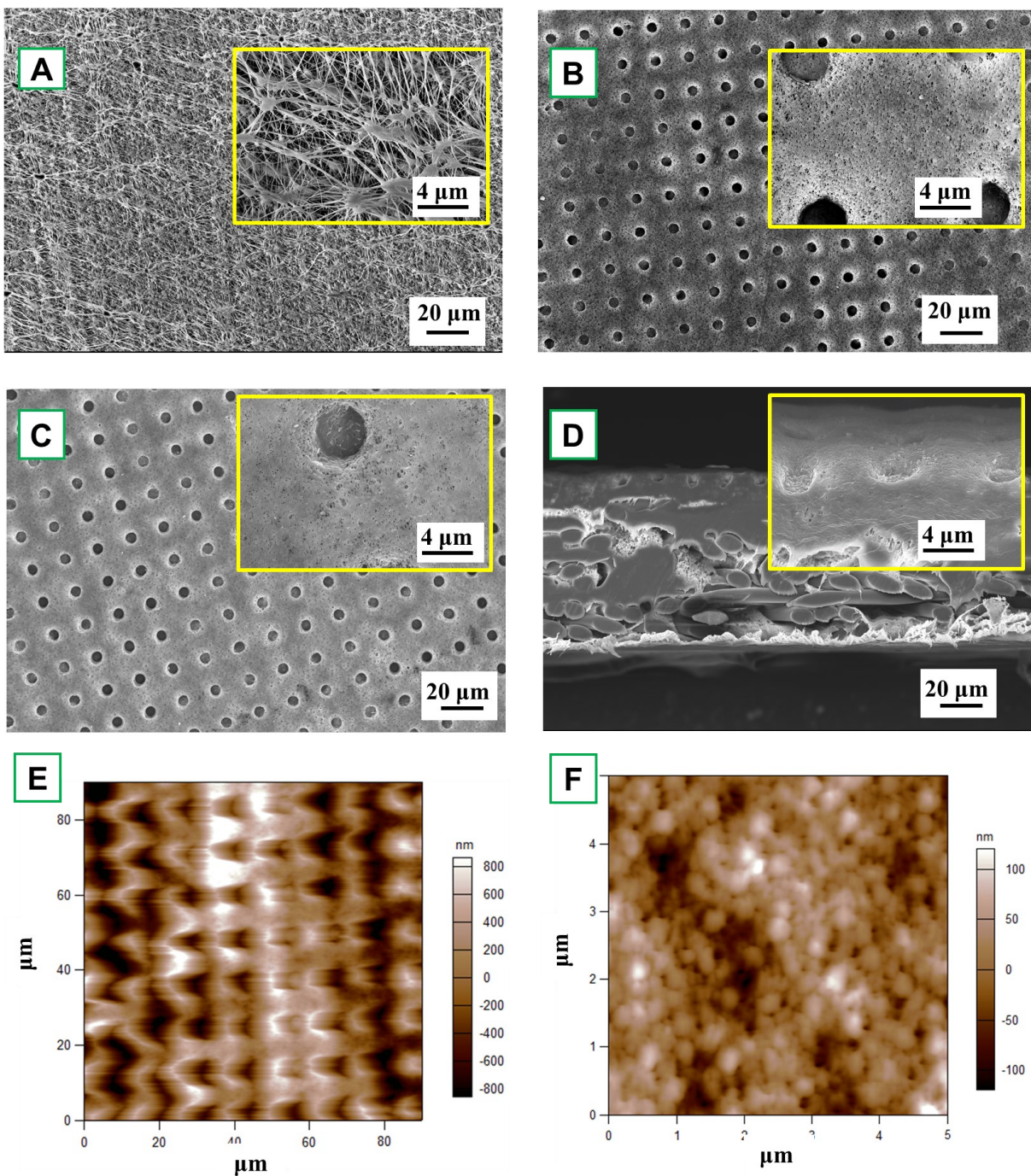
212 3.1 Characteristics of nanofabricated MD membrane.

213 3.1.1 Surface and structural characterization of the nanofabricated MD membrane

214 Commercially available hydrophobic PTFE membrane was chosen as scaffold for the
215 subsequent nanofabrication procedure (Figure 1). PTFE membrane was firstly nanoimprinted
216 and deposited with an ultrathin TiO₂ layer whose thickness was around 5.56 ± 0.11 nm, which
217 was measured from the reference silicon wafer (Figure S2, Supplementary Data). Fiber-like
218 texture of PTFE membrane surface disappeared, and membrane surface manifested a periodic,
219 circular surface pattern. Compared with other coating techniques, atomic layer deposition can
220 realize an extra-uniform TiO₂ layer. As a result, the membrane surface became smoother without
221 obvious agglomerated TiO₂ nanoparticles.

222 A close examination of circular indentation shows elongated features in the vertical
223 dimension, exhibiting hierarchy morphology. Besides, AFM image of TiO₂ deposition
224 membrane (Figure 2E and F) shows the spherical hierarchical structure which might lead to a
225 special wettability, thereby being beneficial to MD separation. After fluorination, there is no
226 significant difference with ALD membrane, only scattered, tiny agglomerated particles could be
227 observed. The FTES membrane still maintained a highly ordered dot pattern with smoother
228 surface (Figure 2C).

229 Despite a series of modifications, the PTFE membrane was not compromised as evident
230 in the cross-section of FTES membrane (Figure 2D), so that the resultant membrane could expect
231 a satisfactory NaCl rejection in the MD filtration. **Indeed, the membrane integrity of modified**
232 **membrane remain uncompromised, which was evident by a 100% NaCl rejection in MD**
233 **filtration.** To re-cap, after modification, nanofabricated PTFE membrane exhibited a periodic,
234 circular surface pattern with spherical hierarchical structure, while no noticeable compromise on
235 membrane structure was observed.



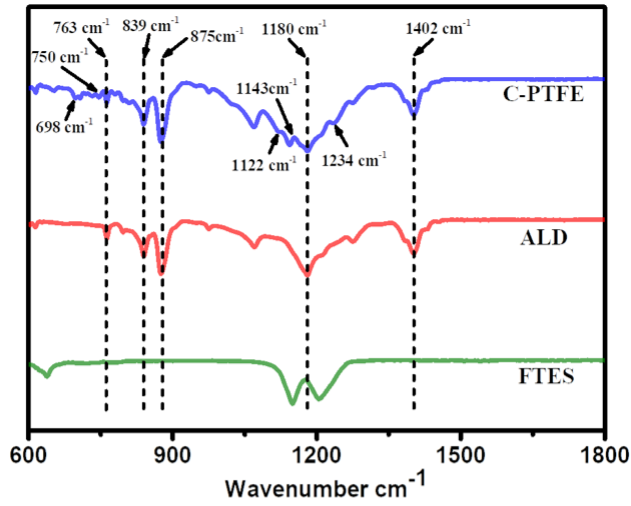
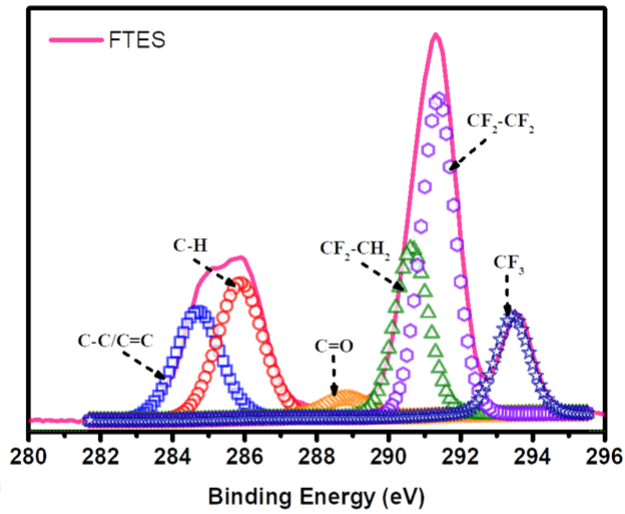
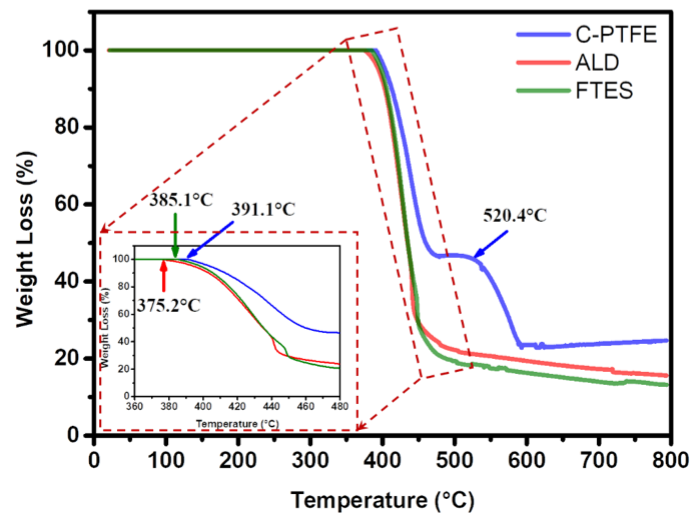
236

237 **Figure 2:** SEM images of membrane surface morphology: (A) pristine PTFE (C-PTFE); (B)
 238 TiO₂ atomic layer deposited nanoimprinted membrane (ALD); (C) fluorinated ALD membrane
 239 (FTES); (D) cross-section of FTES. Atomic Force Microscopy (AFM) imaging of (E) the
 240 membrane surface demonstrating the dot pattern and (F) deposition layer of TiO₂.

241 3.1.2 Chemistry characterization of the nanofabricated MD membrane

242 The surface modification of PTFE membrane with ALD and FTES was determined by
243 ATR-FTIR and XPS, as shown in Figures 3A and 3B. Peak occurrence at wavenumbers of 839
244 and 875 cm^{-1} (red curve) suggests the bonding of TiO_2 nanoparticles onto membrane via ALD
245 deposition. Reacting with anchoring TiO_2 nanoparticles, a fluorosilane surface modification was
246 initiated involving hydrolysis and condensation of alkoxy silane groups with hydroxyl functional
247 groups of the TiO_2 nanoparticles. The completion of this fluorosilane reaction was evident by the
248 peak occurrence at wavenumbers of 1180 cm^{-1} and 1234 cm^{-1} , representing CF_2 and CF_3 bonds
249 (blue curve). Indeed, the C1 scan of the resultant membrane showed the CF_2 - CF_2 and CF_3 bonds
250 on the membrane surface (Figure 3B). More importantly, the occurrence of CF_3 bond is the
251 characteristic functional group possessing low surface energy that is favorable for MD
252 performance, particularly in treatment of streams containing surfactants.

253 The composition of our modified membranes was further studied by thermo-gravimetric
254 analysis (TGA). As shown in Figure 3C, the weight of C-PTFE, ALD and FTES kept stable
255 when the temperature was below $350\text{ }^\circ\text{C}$. After that, the three membranes began to lose weight at
256 $375.2\text{ }^\circ\text{C}$ (ALD), $385.1\text{ }^\circ\text{C}$ (FTES) and $391.1\text{ }^\circ\text{C}$ (C-PTFE), respectively. There was a consistent
257 shift of thermal decomposition towards lower temperature of modified membranes (both ALD-
258 and FTES-modified membranes), which indicates enhancement in thermal stability. Higher
259 residual mass was observed for ALD modified membrane in comparison with FTES modified
260 membrane indicating the dispersion of TiO_2 nanoparticles in the composite membrane that
261 resulted to improved thermal properties. Another feature presented in the TGA diagram was that
262 TiO_2 deposition on the membrane may catalyse more C-PTFE loss.

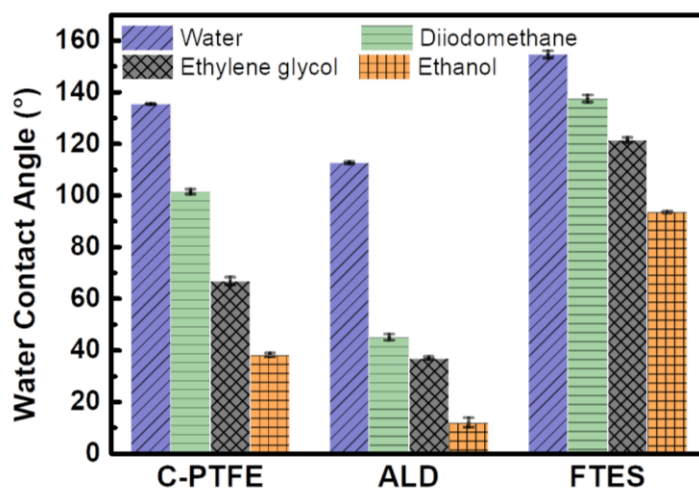
A**B****C**

264 **Figure 3:** Chemistry characterization of C-PTFE, ALD and FTES modified membranes. (A)
265 ATR-FTIR spectra; (B) XPS spectra of C1s of FTES modified membrane; and (C) TGA curves.

266 3.2 Wetting properties of the nanofabricated MD membrane

267 The surface wettability of relevant nanofabricated membranes was measured using static
268 water and low surface tension liquids (diiodomethane, ethylene glycol and ethanol) contact
269 angles as shown in Figure 4. C-PTFE exhibited a high water contact angle of 135°, due to its
270 hydrophobic nature. After the TiO₂ deposition, the contact angle decreased to 112°. TiO₂ can
271 produce oxygen vacancies on its surface, which could be occupied by water molecules and
272 produce adsorbed -OH groups. Thus, the membrane coated by TiO₂ tended to have a more
273 hydrophilic surface, as demonstrated by lower WCA. By contrast, the fluorination by FTES
274 endowed the ALD with extremely high water contact angle of 155°, thereby rendering a low
275 surface energy as well as manifesting excellent hydrophobicity.

276 The ALD deposition created a hierarchically rough nanostructure. Based on the Wenzel
277 and Cassie's theory, establishment of nano/microscale structures was essential for improving the
278 super-hydrophobicity of a membrane. The contact angles of low surface tension liquids had the
279 same tendency with water for similar reasons. As a result, the super-hydrophobic surface of
280 FTES is expected to have a robust stability for MD applications.



281

282 **Figure 4:** Water and low surface tension liquids (diiodomethane, ethylene glycol and ethanol)
283 contact angles of C-PTFE, ALD and FTES modified membranes. Error bars indicate the standard
284 deviation of three repeated measurements from two membrane samples.

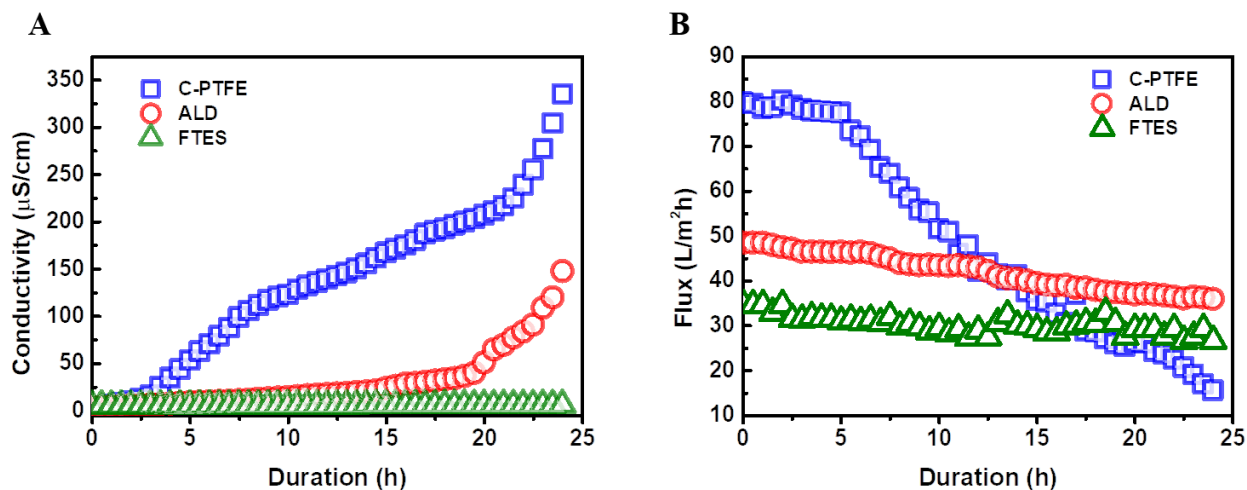
285

286

287 **3.3 Nanofabricated MD membrane exhibited anti-wetting behaviour**

288 To further examine the role of fluorinated, hierarchically rough, nanostructure membrane
289 surface, we compared the wetting behavior of ALD and FTES membranes to the pristine PTFE
290 membrane using saline feed containing 1 mM SDS. The wetting phenomenon was quantified as
291 the increase of permeate conductivity (Figure 5). It was observed that the permeate conductivity
292 of pristine PTFE membrane soared sharply at the beginning, indicating the occurrence of
293 membrane wetting. Although the pristine PTFE membrane is intrinsically hydrophobic, a
294 declining trend in the rejection of NaCl over time was observed, which was consistent with
295 membrane wetting during filtration. By contrast, after TiO₂ ALD modification, the permeate
296 conductivity maintained stable for 20 hours. We attribute it to its hierarchically rough
297 nanostructure. Despite the relatively low water contact angle, the hierarchically rough
298 nanostructure could create air pockets on the membrane surface¹⁹, and thus mitigate membrane
299 wetting. In comparison, FTES modified membrane was able to sustain MD performance. The
300 nanofabricated surface that achieved by fluorination and hierarchically rough nanostructure
301 could successfully preserve a metastable Cassie-Baxter state (liquid-air interface) that prevents
302 the membrane from being wetted³²⁻³⁴.

303 Profiles of water flux during the filtration also confirmed the occurrence of membrane
304 wetting (Figure 5B). The pristine PTFE was subject to a rapid flux decline. More importantly,
305 surfactant in the feed can wick into the membrane pores with ease, preventing the transfer of
306 vapor across the membrane. While the TiO₂ ALD and FTES modified MD membranes could
307 maintain relatively steady water flux. In addition, it was noteworthy that the water flux of the
308 FTES modified membrane (34 Lm⁻²h⁻¹) was lower than TiO₂ ALD membrane (55 Lm⁻²h⁻¹). This
309 difference could be attributed to the fact that the increase in the thickness of the MD membrane
310 slightly increased the resistance of water vapour transmission.

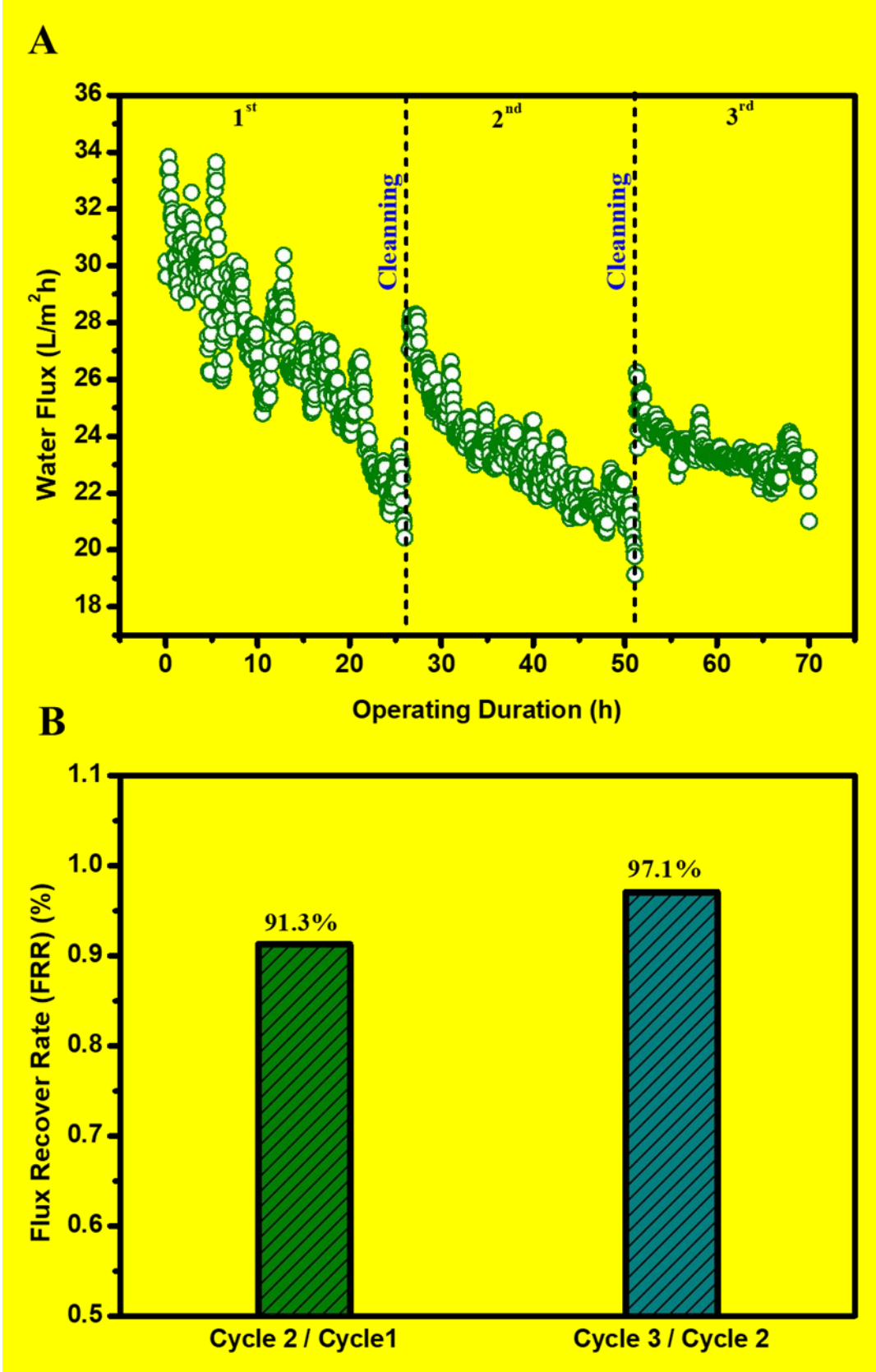


311
 312 **Figure 5:** Comparison of filtration performance of C-PTFE, ALD and FTES modified
 313 membranes: (A) permeate conductivity and (B) water flux.

314

315 **3.4 Nanofabricated MD membrane possessed high fouling reversibility**

316 One important hindrance in deploying MD membrane for challenging waste streams is
 317 membrane fouling and fouling reversibility after cleaning. MD membrane possessing fluorinated
 318 hierarchically rough nanostructure membrane surface was challenged in three fouling-cleaning
 319 cycles where a brief (20 minutes), physical membrane flushing (doubling crossflow velocity)
 320 using DI water was carried out as membrane cleaning. A highly satisfactory water flux recovery
 321 was observed in the second and third cycles, achieving water flux recovery of 91.3% and 97.1%,
 322 respectively (Figure 6b). Such high water flux recovery could be attributed to the nanostructured
 323 surface pattern on the MD membrane. A highly ordered periodic, circular surface pattern can
 324 potentially minimize the foulant-membrane interaction during the filtration. This high fouling
 325 reversibility was consistent with our previous results and recent literature³⁵⁻³⁸. Apart from the
 326 topological perspective, the fluorinated TiO₂ thin film layer on the membrane surface also
 327 renders high slip property (low adhesion) against foulants during filtration. **Indeed, the patterned**
 328 **surface with floriation may alter the foulant deposition from pinned state to suspended state³⁸.**
 329 **Similar observations were also reported in gypsum scaling in MD process by a superhydrophobic**
 330 **micropillared PVDF membrane³⁹.** Both factors contributed to the excellent fouling reversibility,
 331 which is vital for sustainability and robust MD membrane filtration for wastewater treatment.



333 **Figure 6:** Performance of FTES modified membrane in membrane distillation using three
334 fouling-cleaning cycles (A) water flux decline curve; and (B) calculated water flux recovery rate
335 after each cycle. The water flux recovery was calculated as the ratio between initial water fluxes
336 of two consecutive filtration cycles.

337 **4. Conclusion**

338 Results reported here demonstrated a facile and scalable method to fabricate a
339 nanopatterned, omniphobic PTFE membrane via nanoimprinting, atomic layer deposition (ALD),
340 and fluorination for membrane distillation. The nanofabricated MD membrane was imparted
341 with a highly ordered circle pattern and spherical hierarchical rough structure, thereby generating
342 super-hydrophobicity with a water contact angle of 155° and anti-wetting potency for low
343 surface tension liquids. As a result, the nanofabricated MD membrane manifested robust
344 durability with a high and stable water flux around 34 Lm⁻²h⁻¹ for more than 24 hours, and near
345 100% salt rejection in the presence of low surface tension surfactant. More importantly, our
346 modification imparted fouling reversibility, achieving over 91.3% water flux recovery in three
347 fouling-cleaning cycles.

348 **5. Acknowledgements**

349 This work was performed in part at the Melbourne Centre for Nanofabrication (MCN) in
350 the Victorian Node of the Australian National Fabrication Facility (ANFF). R.H. thanked support
351 from China Scholarship Council.

352 **6. References**

- 353 1. Y. Jiang, *Environmental Science & Policy*, 2015, **54**, 106-125.
- 354 2. M. Hanna-Attisha, J. LaChance, R. C. Sadler and A. Champney Schnepf, *American*
355 *journal of public health*, 2016, **106**, 283-290.
- 356 3. F. Boltz, N. L. Poff, C. Folke, N. Kete, C. M. Brown, S. S. G. Freeman, J. H. Matthews,
357 A. Martinez and J. Rockström, *Water Security*, 2019, **8**, 100048.
- 358 4. I. Aselmann and P. Crutzen, *Journal of Atmospheric chemistry*, 1989, **8**, 307-358.
- 359 5. S. K. Hubadillah, M. H. D. Othman, T. Matsuura, M. A. Rahman, J. Jaafar, A. Ismail and
360 S. Z. M. Amin, *Sep. Purif. Technol.*, 2018, **205**, 22-31.
- 361 6. J. Chang, J. Zuo, K.-J. Lu and T.-S. Chung, *Desalination*, 2019, **449**, 16-25.

- 362 7. J. Guo, B. J. Deka, K.-J. Kim and A. K. An, *Desalination*, 2019, **468**, 114054.
- 363 8. A. Alkudhiri, N. Darwish and N. Hilal, *Desalination*, 2012, **287**, 2-18.
- 364 9. R. D. Gustafson, S. R. Hiibel and A. E. Childress, *Desalination*, 2018, **448**, 49-59.
- 365 10. X. An, Z. Liu and Y. Hu, *Desalination*, 2018, **432**, 23-31.
- 366 11. M. Rezaei, D. M. Warsinger, M. C. Duke, T. Matsuura and W. M. Samhaber, *Water Res.*,
367 2018, **139**, 329-352.
- 368 12. K. Li, D. Hou, C. Fu, K. Wang and J. Wang, *Journal of Environmental Sciences*, 2019,
369 **75**, 277-288.
- 370 13. Y. Shao, M. Han, Y. Wang, G. Li, W. Xiao, X. Li, X. Wu, X. Ruan, X. Yan and G. He,
371 *Journal of membrane science*, 2019, **579**, 240-252.
- 372 14. W. Qin, J. Zhang, Z. Xie, D. Ng, Y. Ye, S. R. Gray and M. Xie, *Environmental Science:
373 Water Research & Technology*, 2017, **3**, 119-127.
- 374 15. L. Dumée, V. Germain, K. Sears, J. Schütz, N. Finn, M. Duke, S. Cerneaux, D. Cornu
375 and S. Gray, *Journal of membrane science*, 2011, **376**, 241-246.
- 376 16. M. Tang, D. Hou, C. Ding, K. Wang, D. Wang and J. Wang, *Sci. Total Environ.*, 2019,
377 **696**, 133883.
- 378 17. H. Li, X. Zi, W. Shi, L. Qin, H. Zhang and X. Qin, *Membrane Water Treatment*, 2019,
379 **10**, 287-298.
- 380 18. Y. Liao, G. Zheng, J. J. Huang, M. Tian and R. Wang, *Journal of Membrane Science*,
381 2020, **601**, 117962.
- 382 19. J. Ge, D. Zong, Q. Jin, J. Yu and B. Ding, *Adv. Funct. Mater.*, 2018, **28**, 1705051.
- 383 20. F. Guo, A. Servi, A. Liu, K. K. Gleason and G. C. Rutledge, *ACS applied materials &
384 interfaces*, 2015, **7**, 8225-8232.
- 385 21. Y.-X. Huang, Z. Wang, J. Jin and S. Lin, *Environmental science & technology*, 2017, **51**,
386 13304-13310.
- 387 22. H.-C. Yang, W. Zhong, J. Hou, V. Chen and Z.-K. Xu, *Journal of Membrane Science*,
388 2017, **523**, 1-7.
- 389 23. Y. Liu, T. Xiao, C. Bao, Y. Fu and X. Yang, *Journal of membrane science*, 2018, **563**,
390 298-308.
- 391 24. Z. Zhu, Z. Liu, L. Zhong, C. Song, W. Shi, F. Cui and W. Wang, *Journal of Membrane
392 Science*, 2018, **563**, 602-609.
- 393 25. J. H. Kim, S. H. Park, M. J. Lee, S. M. Lee, W. H. Lee, K. H. Lee, N. R. Kang, H. J. Jo,
394 J. F. Kim and E. Drioli, *Energy & Environmental Science*, 2016, **9**, 878-884.
- 395 26. S. H. Maruf, L. Wang, A. R. Greenberg, J. Pellegrino and Y. Ding, *Journal of membrane
396 science*, 2013, **428**, 598-607.
- 397 27. Z. Zhan and Y. Lei, *ACS nano*, 2014, **8**, 3862-3868.

- 398 28. M. Xie, W. Luo and S. R. Gray, *Water Res.*, 2017, **124**, 238-243.
- 399 29. S. M. George, *Chemical Reviews*, 2010, **110**, 111-131.
- 400 30. R. L. Puurunen, *Journal of Applied Physics*, 2005, **97**, 121301.
- 401 31. Y. Chul Woo, Y. Chen, L. D. Tijing, S. Phuntsho, T. He, J.-S. Choi, S.-H. Kim and H.
402 Kyong Shon, *Journal of Membrane Science*, 2017, **529**, 234-242.
- 403 32. H. Y. Erbil and C. E. Cansoy, *Langmuir*, 2009, **25**, 14135-14145.
- 404 33. J. Lee, C. Boo, W.-H. Ryu, A. D. Taylor and M. Elimelech, *ACS applied materials &*
405 *interfaces*, 2016, **8**, 11154-11161.
- 406 34. A. Sudeepthi, L. Yeo and A. Sen, *Appl. Phys. Lett.*, 2020, **116**, 093704.
- 407 35. Y.-J. Won, J. Lee, D.-C. Choi, H. R. Chae, I. Kim, C.-H. Lee and I.-C. Kim,
408 *Environmental Science & Technology*, 2012, **46**, 11021-11027.
- 409 36. D.-C. Choi, S.-Y. Jung, Y.-J. Won, J. H. Jang, J.-W. Lee, H.-R. Chae, J. Lim, K. H. Ahn,
410 S. Lee, J.-H. Kim, P.-K. Park and C.-H. Lee, *Environmental Science & Technology*
411 *Letters*, 2017, **4**, 66-70.
- 412 37. J. A. Kharraz and A. K. An, *Journal of Membrane Science*, 2020, **595**, 117596.
- 413 38. Z. Xiao, H. Guo, H. He, Y. Liu, X. Li, Y. Zhang, H. Yin, A. V. Volkov and T. He,
414 *Journal of Membrane Science*, 2020, **599**, 117819.
- 415 39. Z. Xiao, Z. Li, H. Guo, Y. Liu, Y. Wang, H. Yin, X. Li, J. Song, L. D. Nghiem and T.
416 He, *Desalination*, 2019, **466**, 36-43.
- 417